Dynamics of the helium atom close to the full fragmentation threshold: Double ionization

C. Bouri,* P. Selles, and L. Malegat
Laboratoire d'Interaction du Rayonnement X Avec la Matière (Laboratoire associé au CNRS), Université Paris–Sud, 91405 Orsay, France

M. G. Kwato Njock
CEPAMOQ, Faculty of Science, University of Douala, P. O. Box 8580 Douala, Cameroon
(Received 7 November 2005; published 28 February 2006)

A complete set of cross sections is presented for photodouble ionization of He at 0.1 eV above the threshold. Special care is taken to clear the asymmetry parameter and the energy differential cross section of any ionization-excitation contribution. As a result, their limiting behaviors for the fully asymmetric partitionings of the excess energy are elucidated, thus shedding light on pending discussions in the field. A reliable scheme follows for computing the fully integrated cross section. Very good agreement is observed between the calculated and measured fully differential cross sections after a detailed reassessment of the experimental normalization procedure. The present findings are compared with the assumptions underlying the Wannier picture of near-threshold double escape.

DOI: 10.1103/PhysRevA.73.022724 PACS number(s): 32.80.Fb

I. INTRODUCTION

Considerable progress has been made in the past few years regarding the description of highly correlated three-body Coulomb systems above their full fragmentation threshold (see [1] for the results up to 2000 and Ref. [2] for more recent work). Our qualitative understanding of the mechanisms underlying double escape (see, for instance, Refs. [3,4]) has advanced in line with our ability to describe this process quantitatively. In this respect, a variety of *ab initio* computational methods are now capable of predicting accurate absolute cross sections at any level of differentiation for the prototypical processes of electron-impact ionization of H or double ionization of He. These methods have been applied within an extended energy domain ranging from a few eV to a few hundreds of eV above the relevant thresholds. On the high-energy side, where the three-body nature of the system has a marginal expression, approximate methods based on a perturbative treatment of electronic correlations can take over (see Ref. [5] for a recent application). On the low-energy side, the theoretical supply remained restricted to the Wannier classical model [6] and its subsequent avatars (see Ref. [1] and references therein for details) up to 2004. Then, converged cross sections were obtained simultaneously both for electron impact ionization of H at 0.01 a.u., using the propagating exterior complex scaling method [7], and for photon impact double ionization of He at 0.1 eV, using the hyperspherical $\mathcal{R}$ matrix method with semiclassical outgoing waves (H$\mathcal{R}$M-SOW) [8]. This opened the way to a critical reassessment of Wannier ideas based on *ab initio* calculations. However, before proceeding any further with the H$\mathcal{R}$M-SOW method, one had to design a practical scheme to unravel the double ionization channel of interest from the infinite series of competing ionization-excitation channels with the highest possible accuracy. The projection scheme demonstrated in Ref. [8] has now led to an optimized, vectorized, and parallelized numerical procedure. Accordingly, we are now able to present a full panorama of the three-body dynamics of He at only 0.1 eV above the double ionization threshold. In a recent paper [9], we have presented cross sections and asymmetry parameters for ionization-excitation leaving the residual ion in levels up to $n=50$. Here, we present the complementary double ionization data, which include a full set of cross sections: $\sigma^5(E;E_1,\Omega_1,\Omega_2)$, which is differential in the emission directions Ω_1 and Ω_2 of the two electrons and in the energy E_1 of one of them, for a given total energy E, will be referred to as the fivefold differential cross section (FDCS); $\sigma^3(E;E_1,\Omega_1)$ will be characterized by the asymmetry parameter $\beta(E;E_1)$ which controls its shape; the energy differential cross section $\sigma^1(E;E_1)$ will be referred to as the singly differential cross section (SDCS); $\sigma^0(E)$ will be referred to as the integrated cross section (ICS).

In Sec. II, we recall the main features of the method and present the numerical procedure used to strip off the successive ionization-excitation channels from the photoionization wave function to get as clean a double ionization wave function as possible. We also present the general form of this wave function, to make the expressions of the cross sections used later on understandable. In Sec. III, we present partly differential cross sections, starting with the asymmetry parameter and the SDCS. A simple procedure allows us to clear these quantities of any remaining ionization-excitation contribution and to derive their limits for the extreme energy sharings $E_1=E$ and $E_1=0$. The ICS follows by integrating the SDCS over half its energy interval of definition. In Sec. IV, we compare our calculated FDCSs with those measured in Ref. [10]. Very good agreement is achieved between theory and experiment after a detailed reexamination of the experimental normalization procedure. All these findings are con-

*Permanent address: CEPAMOQ, Faculty of Science, University of Douala, P. O. Box 8580 Douala, Cameroon.

fronted with the expectations based on previous near-threshold theoretical and experimental work, a review of which can be found in Ref. [11]. The concluding Sec. V summarizes the present contribution and announces further developments.

II. METHOD

The H$\mathcal{R}$M-SOW method proposes a simple scheme to compute the wave function of a helium atom, initially in its ground state $\Psi_0(\vec{r}_1,\vec{r}_2)$ of energy E_0, after it has absorbed a single linearly polarized photon carrying an energy larger than the He double ionization potential. This photoionization wave function, denoted $\overline{\Psi}(\vec{r}_1,\vec{r}_2)$, is obtained by solving the stationary inhomogeneous Schrödinger equation

$$[H-(E_0+\omega)]\overline{\Psi}(\vec{r}_1,\vec{r}_2)=-\frac{1}{2}\vec{\mathcal{E}}\cdot\vec{D}\Psi_0(\vec{r}_1,\vec{r}_2) \tag{1}$$

for an outgoing wave asymptotic condition. In Eq. (1), H denotes the field-free two-electron Hamiltonian, and $\vec{D}$ the dipole operator that couples the atom to the external electric field of amplitude $\vec{\mathcal{E}}$ and frequency ω. This equation is solved in a set of partially collective coordinates which consists of the hyperspherical radius $R=\sqrt{r_1^2+r_2^2}$, the radial correlation angle $\alpha=\tan^{-1}(r_2/r_1)$, and the spherical angles ϑ_1,φ_1, and ϑ_2,φ_2, that specify the directions of the unit vectors $\hat{r}_1$ and $\hat{r}_2$ with respect to the polarization axis z. For convenience, we introduce the compact notations $\Omega_1=\{\vartheta_1,\varphi_1\}$, $\Omega_2=\{\vartheta_2,\varphi_2\}$, and $\Omega=\{\alpha,\Omega_1,\Omega_2\}$. The R^{-1} dependence of the three-body Coulomb potential suggests to separate configuration space into two regions: an inner region, $R\leqslant R_0$, where the R dependence is strong, and a complementary outer region where it is weak enough to support a semiclassical treatment. The fully quantal inner region calculation, based on the $\mathcal{R}$-matrix approach and the adiabatic partial wave analysis, provides the solution $\overline{\Psi}(R_0;\Omega)$ on the hypersphere $R=R_0$. In the outer region, the five-dimensional angular motion is described according to quantum mechanics, whereas the hyperradial motion is treated semiclassically. This brings the solution of Eq. (1) back to a hyperradial propagation problem. The solution extracted at the border R_0 of the inner region is then propagated to a very large distance R_∞ where the cross sections are obtained directly from the relevant outgoing fluxes.

This general scheme, the details of which can be found in previous publications [12–14], is complemented by two different procedures which have been designed to identify the successive ionization-excitation channels and to subtract them from the photoionization wave function Ψ at appropriate hyperradii in the course of the propagation.

The first procedure is based on the expansion of the wave function at R_0 on the adiabatic angular basis defined at this distance. As shown in previous publications (see, for instance, Ref. [15]), groups of adiabatic channels can be associated with ionization-excitation to successive levels of the residual ion, the multiplicity of each group being equal to the first-order Stark degeneracy of the corresponding hydrogenic level of He^+. This procedure is applied here at the border $R=R_0=60$ a.u. of the inner region. Ionization-excitation channels up to and including $n=3$, corresponding to the first nine adiabatic channels, are identified and subtracted from the wave function to propagate. The latter, called $\Psi_3(R_0;\Omega)$, is given accordingly by

$$\Psi_3(R_0;\Omega)=\overline{\Psi}(R_0;\Omega)-\sum_{\lambda=1}^{9}u_\lambda(R_0)Z_\lambda(R_0;\Omega), \tag{2}$$

where $Z_\lambda(R_0;\Omega)$ denote the adiabatic angular partial waves at R_0 and $u_\lambda(R_0)$ the expansion coefficients of $\overline{\Psi}(R_0;\Omega)$ on this locally adapted angular basis.

In the second procedure, the ionization-excitation channel n is described by the projection of the photoionization wave function on the hydrogenic state n of the residual ion, performed at the appropriate hyperradius R_n as explained in Ref. [9]. Denoting P_n the corresponding projector, and $\Psi_{n-1}(R_n;\Omega)$ the current photoionization wave function, cleared of all ionization-excitation channels up to and including $n-1$, we can write the wave function to be propagated beyond R_n as

$$\Psi_n(R_n;\Omega)=(1-P_n)\Psi_{n-1}(R_n;\Omega). \tag{3}$$

This procedure is applied here from $n=4$. Beyond $n=50$, the accuracy of the projection technique deteriorates, so that we can no longer extract reliable ionization-excitation cross sections and asymmetry parameters. Accordingly, beyond R_{50}, we propagate $\Psi_{50}(R_{50};\Omega)$ without subtracting further excitation channels. Noting $\mathcal{P}(R_n,R_{n-1})$ the unitary operator that propagates the wave function from R_{n-1} to R_n, we can then summarize the propagation scheme that is used here by the expression

$$\Psi_{50}(R_\infty;\Omega)=\mathcal{P}(R_\infty,R_{50})\left(\prod_{n=50}^{5}(1-P_n)\mathcal{P}(R_n,R_{n-1})\right)\times(1-P_4)\mathcal{P}(R_4,R_0)\Psi_3(R_0). \tag{4}$$

In the following, it will be shown that the residual ionization-excitation contributions to the final wave function $\Psi_{50}(R_\infty;\Omega)$ are confined within α intervals around $\alpha=0$ and $\alpha=\pi/2$, the width of which is of the order of $\pi/100$. Since $\tan\alpha\simeq\sqrt{E_2/E_1}$ for large R, these values of α correspond to extremely asymmetric sharings of the excess energy, namely $E_2/E_1\leqslant 10^{-3}$ or $E_1/E_2\leqslant 10^{-3}$. Accordingly, the FDCS, SDCS, and β, obtained from Ψ_{50} for energy sharings outside these very restricted ranges, will be *pure double ionization* cross sections and asymmetry parameters. Moreover, a simple procedure will be presented to extrapolate the pure double ionization SDCS and β toward $\alpha=0$ and $\alpha=\pi/2$. Therefore, a full set of accurate double ionization cross sections will be extracted from Ψ_{50} in what follows. Explicit expressions of these cross sections will be given, which depend on the exact form of the final wave function. We thus complete the present section by expliciting Ψ_{50}, which turns out to be the product of three terms: a geometrical factor associated with the volume element in the six-dimensional configuration space, a semiclassical outgoing wave that describes the bulk of the hyperradial motion in terms of an

effective local momentum, and a reduced wave function that depends only weakly on R. We have then

$$\Psi_{50}(R_\infty;\Omega) = \frac{1}{R_\infty^{5/2}\sin 2\alpha}\frac{1}{\sqrt{p(R_\infty,E)}} \times \exp\left(\imath\int_{R_0}^{R_\infty} p(R',E)dR'\right)\Phi(\Omega), \quad (5)$$

where $p(R,E)$ is known from previous publications (see, for instance, Ref. [15]). Note that we call the reduced wave function $\Phi(\Omega)$, omitting its dependence on R_∞ for simplicity. This wave function is obtained in our approach as the following expansion over normalized symmetrized bipolar harmonics ${}^{\epsilon}\mathcal{Y}^{10}_{\ell\ell+1}(\Omega_1,\Omega_2)$:

$$\Phi(\Omega) = \sum_{\ell=0}^{L}\sum_{\epsilon=g,u} c_\ell^\epsilon(\alpha)\,{}^{\epsilon}\mathcal{Y}^{10}_{\ell\ell+1}(\Omega_1,\Omega_2), \quad (6)$$

where $\epsilon=g$ (u) labels functions that are symmetric (antisymmetric) in the exchange of the two electrons. The entire information is then contained in the set of coefficients $c_\ell^\epsilon(\alpha)$ which will enter the expressions of the cross sections in the following sections.

III. PARTLY DIFFERENTIAL AND INTEGRATED CROSS SECTIONS

A. Limiting behavior of β and the SDCS for fully asymmetric energy sharings

The FDCS is obtained from the flux of $\Psi_{50}(R_\infty;\Omega)$ through an elementary surface on the hypersphere $R=R_\infty$. Accordingly, it can be expressed in terms of the reduced wave function as

$$\sigma^5(E;E_1,\Omega_1,\Omega_2) = 2\frac{2\pi\omega}{c}\frac{1}{E\sin 2\alpha}|\Phi(\Omega)|^2. \quad (7)$$

The triply and singly differential cross sections follow by successive integrations. They are given by

$$\sigma^3(E;E_1,\Omega_1) = 2\frac{2\pi\omega}{c}\frac{1}{E\sin 2\alpha}\int d\Omega_2|\Phi(\alpha,\Omega_1,\Omega_2)|^2, \quad (8a)$$

$$\sigma^1(E;E_1) = 2\frac{2\pi\omega}{c}\frac{1}{E\sin 2\alpha}\int d\Omega_1\, d\Omega_2|\Phi(\alpha,\Omega_1,\Omega_2)|^2, \quad (8b)$$

and the asymmetry parameter reads

$$\beta(E;E_1) = \frac{\sqrt{20\pi}}{\sigma^1(E;E_1)}\int d\Omega_1\, Y_{20}^*(\Omega_1)\sigma^3(E;E_1,\Omega_1). \quad (9)$$

Taking account of Eq. (6), one can rewrite these expressions more conveniently as

$$\sigma^1(E;E_1) = 2\frac{2\pi\omega}{c}\frac{1}{E\sin 2\alpha}D_g(\alpha), \quad (10a)$$

$$\beta(E;E_1) = \frac{N_g(\alpha)+N_u(\alpha)}{D_g(\alpha)}, \quad (10b)$$

the new functions introduced being given in terms of the expansion coefficients of the reduced wave function by

$$D_g(\alpha) = \sum_{\ell=0}^{L}(|c_\ell^g|^2+|c_\ell^u|^2), \quad (11a)$$

$$N_g(\alpha) = \sum_{\ell=0}^{L}\frac{2\ell^2+4\ell+3}{4\ell^2+8\ell+3}(|c_\ell^g|^2+|c_\ell^u|^2) - \sum_{\ell=0}^{L-1}3\frac{\sqrt{\ell^2+3\ell+2}}{2\ell+3}\mathrm{Re}(c_\ell^g c_{\ell+1}^{g*}-c_\ell^u c_{\ell+1}^{u*}), \quad (11b)$$

$$N_u(\alpha) = -\sum_{\ell=0}^{L}6\frac{\ell+1}{4\ell^2+8\ell+3}\mathrm{Re}(c_\ell^g c_\ell^{u*}) + \sum_{\ell=0}^{L-1}3\frac{\sqrt{\ell^2+3\ell+2}}{2\ell+3}\mathrm{Re}(c_\ell^g c_{\ell+1}^{u*}-c_\ell^u c_{\ell+1}^{g*}). \quad (11c)$$

The advantage of introducing the functions above lies in their symmetry properties and limiting behaviors. First of all, they are either symmetric (D_g,N_g) or antisymmetric (N_u) in the exchange of the two electrons. Accordingly, Eqs. (10) make clear that $\sigma^1(E,E_1)$ is symmetric in this operation, whereas $\beta(E,E_1)$ is neither symmetric nor antisymmetric. But more importantly, their limiting behavior at the edges of the α interval is known. They tend toward zero to allow $\sigma^1(E,0)$, $\beta(E,0)$, and $\beta(E,E)$ to take finite values, which are given indeed by

$$\sigma^1(E,0) = \sigma^1(E,E) = \frac{2\pi\omega}{cE}D_g'(0),$$

$$\beta\left(E,\frac{0}{E}\right) = \frac{N_g'(0)\pm N_u'(0)}{D_g'(0)}. \quad (12)$$

The functions D_g,N_g, and N_u, as calculated from Eqs. (11), are displayed in Fig. 1. As the extreme energy sharings are approached, they first tend toward zero as expected. Yet a different behavior sets in at about $\pi/100$ rad from the edges, namely strong and rapid oscillations occur, due to the ionization-excitation channels $n\geqslant 50$ which have not been projected out of the propagated wave function. However, our knowledge of the physical behavior of the D_g, N_g, and N_u functions makes it easy to get rid of this unwanted contribution. All one has to do is to fit the calculated gerade (ungerade) functions, over the reduced interval $[\pi/100,(\pi/2)-(\pi/100)]$ where they are uncontaminated by single escape channels, by even (odd) polynomials in the variable $(\alpha-\pi/4)$, designed to vanish at the edges $\alpha=0$ and $\pi/2$. The best fits are plotted in Fig. 1. They are used to reconstruct a singly differential cross section and a β parameter free of any residual ionization-excitation contribution, which there-

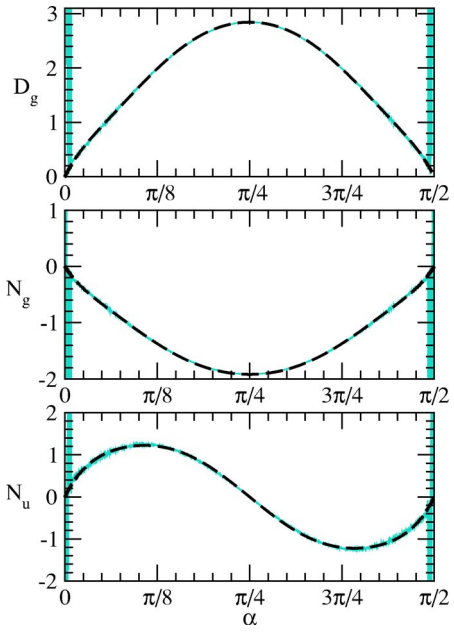

FIG. 1. (Color online) Building blocks of the energy differential cross section and asymmetry parameters in a.u. as a function of the radial correlation angle α in radians. Thin blue continuous line: raw calculation; thick black dashed line: best polynomial fit satisfying the boundary conditions at $\alpha=0$ and $\pi/2$.

fore exhibit the correct physical behavior for the extreme energy sharings.

B. Continuity between ionization with excitation to discrete levels and double ionization

The reconstructed energy differential cross section is plotted in Fig. 2. Its limit for the extreme energy sharings $E_1/E=0$ or $E_1/E=1$ is emphasized by arrows. It is notably different from the limit derived in Ref. [9] by extrapolating

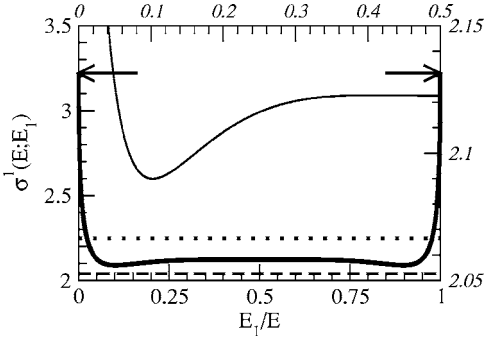

FIG. 2. Reconstructed energy differential cross section in kb/eV shown in two views. Thick continuous line: full view, referred to the left vertical and bottom horizontal axis. Thin continuous line: partial view, referred to the right vertical and top horizontal axis. The arrows point to the limits of the reconstructed SDCS for $E_1=0$ or $E_1=E$. The dotted horizontal line indicates the limit of $n^3\sigma_n(E)/Z^2$ as $n\to\infty$ as extracted from ionization-excitation data in Ref. [9]. The dashed horizontal line indicates the limit of $\delta_n(E)\sigma_n(E)$ as $n\to\infty$ as extracted from ionization-excitation data (see text).

ionization-excitation data: the latter, represented by the dotted line, lies indeed much closer to $\sigma_1(E;E/2)$ than to $\sigma_1(E;E)$. This has prompted us to reconsider the conjecture expressed by Eq. (40) of Ref. [9].

The continuity between the discrete and the continuum part of the photoabsorption spectrum of H is well established [16]. It can be expressed quantitatively in terms of the oscillator strengths per unit energy for excitation to discrete and continuum states as

$$\lim_{n\to\infty}\frac{dn}{dE_n}f_n=\lim_{E\to I}\frac{df_E}{dE}, \tag{13}$$

where I denotes the ionization threshold (see, for instance, [17] for a detailed derivation of this relation). Such a continuity is expected between photoionization with excitation and photodouble ionization as well. Yet giving it a quantitative expression is not a trivial task. To our knowledge, the only case in which it has been performed rigorously is that of a fixed photon energy far above the double ionization threshold [18,19]. In this case, electronic correlations are very weak, and the excess energy above each threshold can be considered as constant regardless of the channel considered. In these circumstances, the continuum electron that takes away the whole excess energy can be considered a spectator and Eq. (40) of Ref. [9] appears as a natural extension of Eq. (13). These simplifications, however, disappear at 0.1 eV above the threshold, where electronic correlations are strong, and where the excess energy above each threshold varies significantly from one channel to the other. Accordingly, we are not surprised to note that, at this very low energy, extrapolating ionization-excitation data using Eq. (40) of Ref. [9] does not yield the expected double ionization limit given by Eq. (12). Note in this respect that the n^{-3} dependence of σ_n, implied by Eq. (40) of Ref. [9], has already been questioned [20] on the basis of extensions of the energy differential expression of the Wannier law [21,22]. These extensions, motivated by the symmetric cusp observed in threshold photoelectrons spectra at the double ionization threshold, suggest the following improved version of Eq. (40) of [9]:

$$\lim_{n\to\infty}[\delta_n(E)\times\sigma_n(E)]=\sigma^1(E;E),$$
$$\text{where}\quad \delta_n(E)=\left(1+\frac{Z^2}{n^2E}\right)^{-0.056}\frac{n^3}{Z^2}. \tag{14}$$

The curve representing $\delta_n(E)\sigma_n(E)$ as a function of n, plotted in Fig. 3, must be compared with its counterpart in Fig. 8 of Ref. [9]. It evidences a stabilization at about 2.04 kb/eV from $n=12$, compared to 2.25 kb/eV from $n=10$ in Ref. [9]. More importantly, this stabilization persists up to $n=50$ to a significantly better approximation than in Ref. [9], no steady decay being observed as n increases. This confirms that Eq. (14) incorporates some additional physics compared to Eq. (40) of [9]. Accordingly, we consider the value of 2.04 kb/eV, indicated by a dashed horizontal line in Fig. 2, as an improved extrapolation of ionization-excitation data. However, it still lies much closer to $\sigma_1(E;E/2)$ than to $\sigma_1(E;E)$, just like the less accurate value derived in Ref. [9].

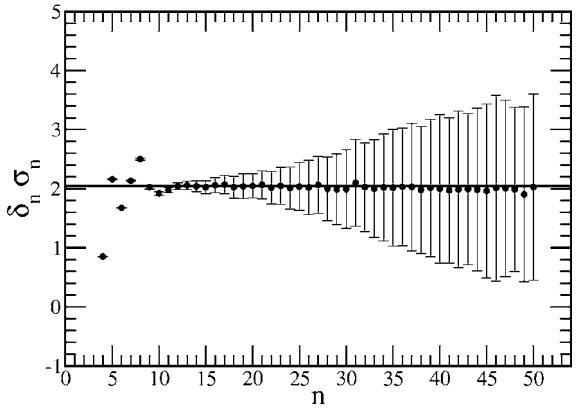

FIG. 3. Extrapolating the ionization-excitation cross sections to infinite n. Dots with error bars: calculated values of $\delta_n(E)\sigma_n(E)$ (in kb/eV); horizontal line: best constant fit (see text).

Thus, the modified conjecture expressed by Eq. (14) is still incorrect.

The reconstructed asymmetry parameter is displayed in Fig. 4. Its limits for the extreme energy sharings $E_1/E=0$ and $E_1/E=1$ are emphasized by arrows. It turns out that $\beta(E;E)$ is close to the value obtained by extrapolating ionization-excitation data in Ref. [9], represented by the dotted line. However, shortly after Ref. [9] was published, we found a more convincing extrapolation method for the asymmetry parameter. The latter is based on the analysis of the cross sections and asymmetry parameters for ionization-excitation in terms of parabolic states of the residual ion, the direction of the ionized electron being taken as the reference axis [23]. The resulting extrapolated asymmetry parameter, represented by the dashed horizontal line at −0.71, lies significantly far from the expected $\beta(E;E)$. We consider this result as an indication that the conjecture expressed by Eq. (41) of Ref. [9] must be reconsidered at low energy.

In fact, the best extrapolated values of the ionization-excitation data, namely $\beta_\infty(E)=-0.71$ and $\delta_\infty(E)\sigma_\infty(E)=2.04$ kb/eV, turn out to be very close to their double ionization counterparts *averaged over all energy partitionings*.

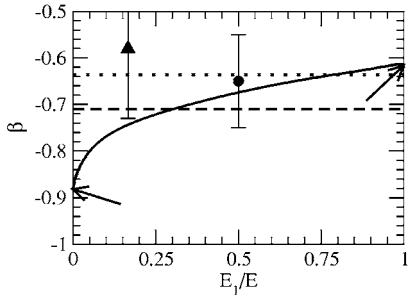

FIG. 4. Asymmetry parameter. Continuous curve: present reconstructed asymmetry parameter. The arrows point to the limits of the reconstructed β for $E_1=0$ or $E_1=E$. Dotted horizontal line: the limit of $\beta_n(E)$ as $n\to\infty$ as extracted from ionization-excitation data in Ref. [9]. Dashed horizontal line: the limit of $\beta_n(E)$ as $n\to\infty$ as extracted from ionization-excitation data in Ref. [23]. Full circle with error bar: measurement [10]. Full triangle with error bar: measurement [29].

The latter indeed are given by $\overline{\sigma}^1(E)=2.13$ kb/eV and $\overline{\beta}(E)=-0.69$. Our results, therefore, suggest a new picture of the merging of ionization-excitation into double ionization, appropriate to the low-energy domain: in this picture, ionization excitation data merge, for infinite n, into their double ionization counterparts *averaged over all possible sharings of the available energy*.

C. Comparison of the calculated SDCS and β with previous experimental and theoretical results

In the absence of experimental investigations, the shape of the SDCS close to the double ionization threshold has been the subject of numerous theoretical studies. Early calculations [24] following the pioneering work of Wannier [6] assumed an essentially flat pattern, a hypothesis that was retained in many subsequent calculations [25]. Later on, classical trajectory studies performed within the Wannier approach [21,22,26] produced a more detailed picture: it was recognized that for excess energies below a few eV, the SDCS should present a positive curvature, the more so the lower the energy. This trend was readily confirmed by first quantum-mechanical *ab initio* calculations [27,28], although the latter were performed at higher energies. Looking at the magnified view of the SDCS given in Fig. 2, we note that our calculations start from a local maximum at 2.12 kb/eV for equal energy sharing, then decrease slowly down to a local minimum of 2.09 kb/eV for $E_1/E\simeq 0.1$, in agreement with the expectations based on these latter calculations. However, for more asymmetric energy sharings, the calculated SDCS increases again up to the limiting value of 3.225 kb/eV. Given the care we have taken to eliminate ionization-excitation contributions, we believe that this unexpected pattern cannot be attributed to spurious contributions from these two-body channels. The only previous *ab initio* calculation performed at excess energies below 1 eV is a recent one that focuses on the threshold behavior of the electron impact ionization cross sections of H [7]. Interestingly, a behavior similar to the one reported here is observed in the SDCS obtained by these authors at 0.01 a.u. Namely, instead of decreasing steadily as the asymmetry increases, their cross section clearly flattens out for $E_1/E\leqslant 0.15$.

There are only two measurements of the asymmetry parameter in the energy region that is of interest here. One [29] yields a β parameter of -0.58 ± 0.15 for a photoelectron carrying less than 20 meV kinetic energy out of 120 meV excess energy above the double ionization threshold. This value compares well with the high-energy limit ($E_1=E$) of the present calculations, whereas it was intended to provide an estimate of the opposite limit ($E_1=0$). By contrast, the experiment [10] provides a value of the equal energy sharing parameter at 0.1 eV excess energy, which is in perfect agreement with the present calculations.

On the theoretical side, early approaches following Wannier's scheme assumed that the asymmetry parameter was independent of the partitioning of the excess energy between the two electrons (see, for instance, Ref. [30]). However, it was shown later on [31] using a more refined treatment that this view was oversimplified and that the partitioning of the

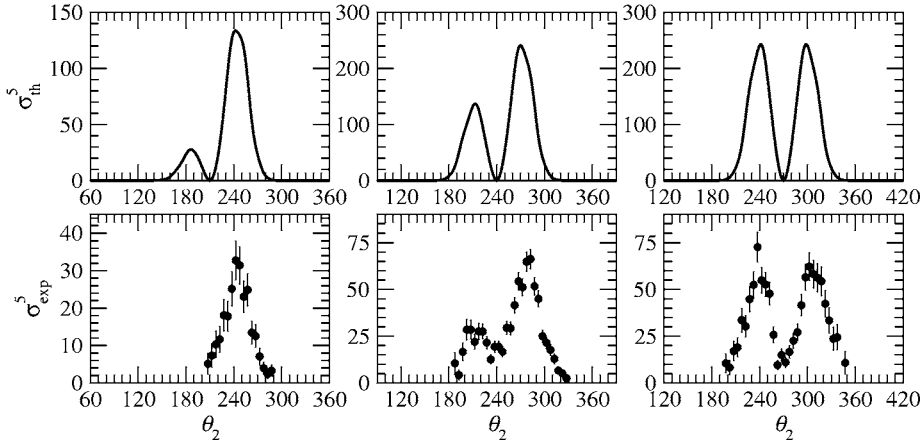

FIG. 5. FDCS (b/eV/sr^2) as a function of the polar angle θ_2 of the second electron in the detection plane (degrees) for the three coplanar geometries investigated in Ref. [10]: $\vartheta_1=30°, 60°, 90°$ from left to right. Top row: present calculation, raw result. Bottom row: original measurements [10].

energy could play a significant dynamical role, notably when approaching threshold. In addition, the two-dimensional function $\beta(E;E_1)$ computed in the 3C model of Ref. [31] was found to have a minimum along $E_1=E/2$. The measurements [32] were first taken as a confirmation of these predictions. Yet the authors in Ref. [32] made the assumption that the double ionization part of photoelectron kinetic energy spectra taken at fixed photon energy and fixed angle was symmetric with respect to $E_1=E_2=E/2$ whatever the angle. Since this holds only at the magic angle [40], their asymmetry parameters appeared wrongly symmetric in the energy sharing with a minimum at equal sharing. In fact, if the dependence of β on the energy sharing can be considered as confirmed by this experiment, this is not so as regards the existence of a minimum at equal sharing. In other respects, a completely different approach, exploiting the symmetry properties of doubly excited states [33], led to the prediction that the double ionization asymmetry parameter corresponding to the slow electron should reach -1 at threshold. The present results shed light on this discussion. First of all, they show that the asymmetry parameter retains a significant dependence on the energy sharing even close to threshold. In addition, this parameter is neither symmetric nor antisymmetric with respect to $E_1/E=0.5$, due to the ungerade coefficients c^u_ℓ which would be neglected in Wannier-type models. Moreover, the asymmetry parameter has a minimum when the detected electron has zero energy, opposite to what was observed in Ref. [31]. This is consistent with the basic classical picture stating that the force exerted by each electron on the other within a pair alters the linear momenta of both, this alteration being more important, on the relative scale, for the slow electron. Finally, the very low value of this minimum, -0.88, confirms the prediction made in Ref. [33].

D. Integrated cross section

Two methods were proposed in Ref. [8] to derive the integrated cross section for photodouble ionization from H$\mathcal{R}$M-SOW calculations: Integrating the SDCS over half the energy interval where it is defined, or subtracting the ionization-excitation cross sections from the total (single +double) ionization cross section. Each of these methods had its drawbacks: in the first one, the SDCS was cleared of spurious ionization-excitation contributions in a somewhat arbitrary way; on the other side, the second method implied extrapolating the ionization-excitation cross sections to infinite values of n, which was a delicate task. At this stage, however, we had no serious doubts regarding the n^{-3} law which was taken as a rule to extrapolate, and accordingly, we recommended the second method. The present experience has reversed our views. Not only do we own now a reliable procedure that produces a pure double ionization SDCS, we also have shown that the n^{-3} law was not verified accurately. As a result, we now recommend the first method. Integrating the reconstructed SDCS of Fig. 2 over the energy interval $[0,E/2]$, we thus get $\sigma^0_{th}=0.107$ kb, to be compared with $\sigma^0_K=0.091\pm0.008$ kb from the reference measurements [34]. The computed value thus lies 0.008 kb above the top of the experimental error bar. Retaining this mismatch as an upper

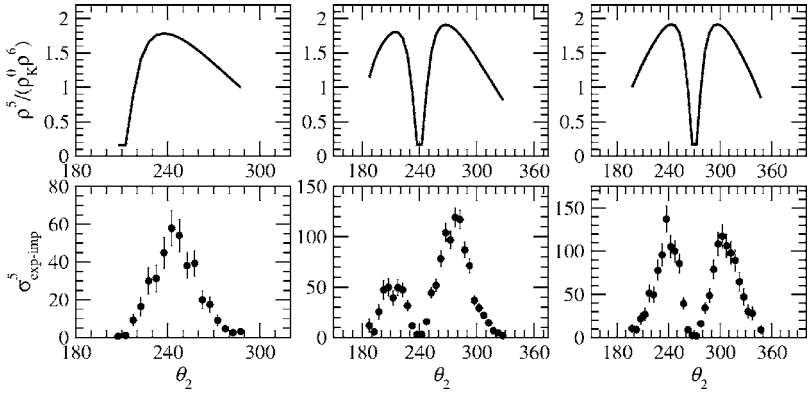

FIG. 6. Normalization of the experimental FDCS. Top row: dimensionless corrective factor to apply to the original data [10]. Bottom row: experimental FDCS deduced from the improved normalization procedure. Units as in Fig. 5.

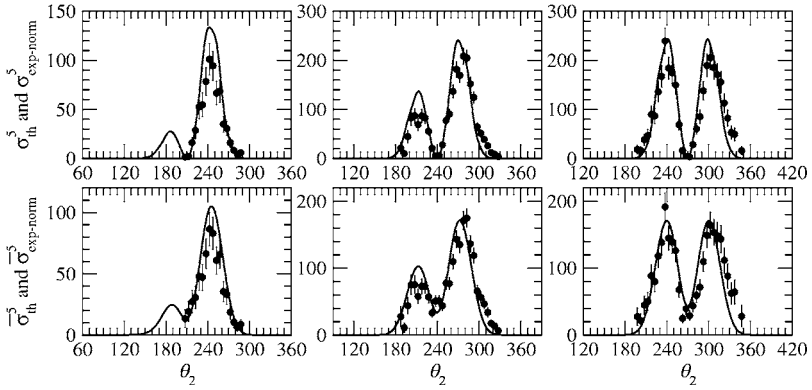

FIG. 7. Comparison between measured and calculated FDCS. Top row: Full line$=\sigma^5_{\text{th}}$; full circles with error bars$=\sigma^5_{\text{exp-norm}}$ deduced from Ref. [10] (see text). Bottom row: Full line$=\overline{\sigma}^5_{\text{th}}$; full circles with error bars$=\overline{\sigma}^5_{\text{exp-norm}}$ deduced from Ref. [10] (see text). Units as in Fig. 5.

bound to the absolute uncertainty attached to the theoretical result, we get a maximum relative uncertainty of the order of 7%. This can be considered very satisfying given the challenge theory must face: extracting a double ionization contribution of the order of 10^{-1} kb from a total ionization cross section of the order of 730 kb [35] with a precision better than 10^{-2} kb. Forthcoming tests of the Wannier threshold law for the ICS will be based on the numerical scheme just outlined.

IV. FIVEFOLD DIFFERENTIAL CROSS SECTION (FDCS)

A. An apparent disagreement between theory and experiment

The FDCS was expressed in terms of the reduced wave function in Eq. (7). Using Eq. (6) and the relations

$$ {}^{g}\mathcal{Y}^{10}_{\ell\ell+1}(\Omega_1,\Omega_2) = \frac{\sqrt{6}}{8\pi}(\cos\vartheta_1+\cos\vartheta_2) \times(-1)^{\ell}\sqrt{\ell+1}P^{01}_{\ell}(\cos\vartheta_{12}), \quad (15a) $$

$$ {}^{u}\mathcal{Y}^{10}_{\ell\ell+1}(\Omega_1,\Omega_2) = \frac{\sqrt{6}}{8\pi}(\cos\vartheta_1-\cos\vartheta_2) \times(-1)^{\ell+1}\sqrt{\ell+1}P^{10}_{\ell}(\cos\vartheta_{12}) \quad (15b) $$

given in Ref. [36], we can recast it now into the convenient form

$$ \sigma^5(E;E_1,\Omega_1,\Omega_2) = \left|(\cos\vartheta_1+\cos\vartheta_2)A_g(\Omega) + (\cos\vartheta_1-\cos\vartheta_2)A_u(\Omega)\right|^2, \quad (16) $$

which was predicted in Ref. [30]. The so-called dynamical factors A_g and A_u are then given by

$$ A_g(\Omega) = \sqrt{\frac{3\omega}{8\pi cE\sin 2\alpha}}\sum_{\ell}(-1)^{\ell}\sqrt{\ell+1}P^{01}_{\ell}(\cos\vartheta_{12})c^{g}_{\ell}(\alpha), \quad (17a) $$

$$ A_u(\Omega) = \sqrt{\frac{3\omega}{8\pi cE\sin 2\alpha}}\sum_{\ell}(-1)^{\ell+1}\sqrt{\ell+1} \times P^{10}_{\ell}(\cos\vartheta_{12})c^{u}_{\ell}(\alpha), \quad (17b) $$

where ϑ_{12} is the mutual angle of the two electrons.

The radiation used in the experiment [10] was characterized by a Stokes parameter $S_1=0.95$. We have checked that assuming pure linear polarization ($S_1=1$) does not alter the results in any visible way. We have thus pursued the analysis in this approximation, the FDCSs being then given directly by Eqs. (16) and (17). They have been calculated for the three coplanar [37] kinematics investigated experimentally in Ref. [10], that is to say $E=100$ meV, $E_1=50$ meV, $\varphi_{12}=\varphi_1-\varphi_2=0^\circ$, and $\vartheta_1=30^\circ, 60^\circ$, and 90°. They are displayed in the first row of Fig. 5 as functions of the polar angle θ_2 of the second electron in the detection plane (to be distinguished from the polar spherical angle ϑ_2), the experimental results [10] being reproduced in the second row. The absolute scales in these two rows are very different: for instance, the calculated cross section σ^5_{th} at $\theta_1=90^\circ$ is close to 240 b/(eV/sr^2) at its highest point, compared to hardly 75 b/(eV/sr^2) for its experimental counterpart σ^5_{exp}. This is not completely unexpected: in Ref. [10] indeed, the authors focused on the shapes of the angular patterns, the absolute scale being proposed only tentatively, and the possibility of an underestimation of the cross section being acknowledged. Careful re-examination of the experimental normalization procedure is thus needed before a meaningful comparison between experiment and theory can be attempted.

B. Enforcing the self-consistency of the experimental normalization procedure

The procedure used in Ref. [10] is based on the relation

$$ \frac{N^5(E;E_1,\vartheta_1,\varphi_1,\vartheta_2,\varphi_{12})}{N^0(E)} = \frac{\sigma^5(E;E_1,\vartheta_1,\varphi_1,\vartheta_2,\varphi_{12})}{\sigma^0(E)} \quad (18) $$

between the numbers of double ionization events recorded in an ideal experiment and the corresponding physical cross sections. This relation allows one to derive the absolute FDCS using any well established reference for the absolute ICS. In the low-energy range, it is usual to rely upon the parametrization $\sigma^0_K(E)=1.02\,E^{1.05}$ given in Ref. [34], where E is in eV and σ^0_K in kb.

In any real experiment, however, the spectral profile of the photon beam has a nonzero width. Accordingly, the measured $N^0(E)$ results from a convolution of the ICS with this

spectral profile. In addition, the time and space resolution of the detectors is finite. The measured $N^5(E;E_1,\vartheta_1,\varphi_1,\vartheta_2,\varphi_{12})$, therefore, takes account of all events characterized by a sextuplet of kinematic parameters $(E';E_1',\vartheta_1',\varphi_1',\vartheta_2',\varphi_{12}')$ located within a finite six-dimensional volume element surrounding the reference point. Moreover, when the statistics is very low, it may be convenient to increase it artificially: for instance, by accumulating the detected events over energy and angular intervals larger than those determined by the resolutions of the experimental devices; or else by adding together all distinguishable events which are known to yield identical cross sections, like those differing only in the value of the absolute azimuthal angle φ_1. Finally, it may also be desirable to discard some series of events, for instance those corresponding to kinematics which lead to deteriorated resolutions. Thus, after reexamining the conditions of Ref. [10] with one of the authors [38], it appeared realistic to rewrite Eq. (18) as

$$\frac{N^5(E;E_1,\vartheta_1,\varphi_1,\vartheta_2,\varphi_{12})}{N^0(E)}=\frac{\int dV^6\sigma^5(E';E_1',\vartheta_1',\varphi_1',\vartheta_2',\varphi_{12}')\mathcal{G}(E';E,\Delta E)\mathcal{H}(E'-E_1'-E_c)}{\int_{-\infty}^{+\infty}\sigma^0(E')\mathcal{G}(E';E,\Delta E)dE'},\tag{19}$$

where $\int dV^6$ is a shortened notation for the six-dimensional integration

$$\int dV^6=\int_{\vartheta_1-(\Delta\vartheta_1/2)}^{\vartheta_1+(\Delta\vartheta_1/2)}\sin\theta_1'd\theta_1'\int_0^{2\pi}d\varphi_1'\int_{\vartheta_2-(\Delta\vartheta_2/2)}^{\vartheta_2+(\Delta\vartheta_2/2)}\sin\theta_2'd\theta_2'\int_{\varphi_{12}-(\Delta\varphi_{12}/2)}^{\varphi_{12}+(\Delta\varphi_{12}/2)}d\varphi_{12}'\int_{E_1-(\Delta E_1/2)}^{E_1+(\Delta E_1/2)}dE_1'\int_{-\infty}^{+\infty}dE'.\tag{20}$$

In Eq. (19), $\mathcal{G}(E';E,\Delta E)$ is a Gaussian function of width $\Delta E=135$ meV, centered at $E=100$ meV, normalized to ensure that $\int_{-\infty}^{+\infty}dE'\mathcal{G}(E';E,\Delta E)=1$. It represents the spectral profile of the photon beam. $\mathcal{H}(E-E_1-E_c)$ is a Heaviside function. It simulates the elimination of electrons having an energy less than the critical value $E_c=20$ meV, below which the angular resolution deteriorates rapidly. Finally, the energy and angular integration ranges in Eq. (20) are as follows: $\Delta E_1=60$ meV, $\Delta\vartheta_1=\Delta\vartheta_2=20°$, and $\Delta\varphi_{12}=40°$.

In Ref. [10], however, it is assumed as usual [39] that the width ΔE of the Gaussian is negligible and that σ^5 and the sine functions in Eq. (19) can be taken out of the integral $\int dV^6$. The experimental FDCS σ_{exp}^5 is then defined by

$$\sigma_{\text{exp}}^5=\frac{\sigma_K^0}{\Delta V_{\text{exp}}^6}\times\frac{N^5}{N^0}\quad\text{where}\quad\Delta V_{\text{exp}}^6=2\pi\sin\vartheta_1\Delta\vartheta_1\sin\vartheta_2\Delta\vartheta_2\Delta\varphi_{12}\Delta E_1.\tag{21}$$

In addition, the authors report that it is reproduced very satisfactorily within the Wannier model by the expression

$$\sigma_{\text{exp}}^5(E;E_1,\vartheta_1,\varphi_1,\vartheta_2,\varphi_{12})=a_{\text{exp}}(E)(\cos\vartheta_1+\cos\vartheta_2)^2\exp\left\{-4\ln 2\left(\frac{\vartheta_{12}-\pi}{\Gamma_{\text{exp}}(E)}\right)^2\right\}\tag{22}$$

with $\Gamma_{\text{exp}}(E)=57\pm4°$ and $a_{\text{exp}}(E)=0.590$ kb/(eV$\times$sr^2) for $E=0.1$ eV. This suggests a very simple consistency check of the entire procedure: integrating Eq. (22) over E_1 and the four angular variables at fixed E should indeed give the reference ICS back. Interestingly, this is not the case, as this integration yields a cross section of 0.041 kb, which is too small by a factor 2.2 since $\sigma_K^0=0.091$ kb. This mismatch reveals that either the normalization procedure (21), or the Wannier model (22), or both, are inaccurate. To clear this point, we have fitted Eq. (22) to our theoretical FDCS at $\vartheta_1=90°$, thus obtaining $a_{\text{th}}=2.55$ kb/(eV$\times$sr^2) and $\Gamma_{\text{th}}=50°$, which after integration yields a total cross section of 0.110 kb, in fair agreement with our exact value of 0.107 kb. Accordingly, the observed lack of self-consistency results from the failure of the usual normalization procedure (21) in the extreme conditions of the experiment [10].

In an attempt to improve this procedure, let us then introduce the averaged FDCS $\overline{\sigma}^5$, the averaged ICS $\overline{\sigma}_K^0$, the exact volume element ΔV^6,

$$\overline{\sigma}^5=\frac{\int dV^6\sigma^5\mathcal{G}\mathcal{H}}{\int dV^6\mathcal{G}\mathcal{H}},\quad\overline{\sigma}_K^0=\int_{-\infty}^{+\infty}dE'\,\sigma_K^0\mathcal{G}\quad\text{and}$$

$$\Delta V^6=\int dV^6\mathcal{G}\mathcal{H},\tag{23}$$

as well as the ratios $\rho^5=\sigma^5/\overline{\sigma}^5$, $\rho_K^0=\sigma_K^0/\overline{\sigma}_K^0$, and $\rho^6=\Delta V^6/\Delta V_{\text{exp}}^6$. Rewriting Eq. (19) in terms of these ratios and using Eq. (21), we can define an improved experimental FDCS by

$$\sigma_{\text{exp-imp}}^5=\sigma_{\text{exp}}^5\frac{\rho^5}{\rho_K^0\rho^6}.\tag{24}$$

We have evaluated the ratios ρ_K^0, ρ^6, and ρ^5, numerically. It turns out that $\rho_K^0\simeq0.98$ provides a negligible correction. As

to ρ^6, it is the product of an angular contribution, which amounts to 0.99 for all geometrical arrangements considered in Ref. [10], and a contribution of 0.69 coming from the energy resolutions. This yields the very important corrective factor $\rho^6 \simeq 0.68$ for all angular distributions measured in Ref. [10]. The evaluation of the last factor ρ^5 required some parametrization of the FDCS. We have used the Wannier model (22) with $\Gamma(E)=67.6E^{0.074}$ and $a(E)=0.783E^{-0.217}$, E being in eV, Γ in degrees, and a in kb/(eV$\times$sr^2). These parametrizations of the energy dependence of the width and amplitude reproduce the Γ values of 57° and 60° measured at 0.1 and 0.2 eV, respectively [10], and ensure that the fivefold integration of Eq. (22) yields the reference ICS σ_K^0 back at these two energies. In this model, the resulting ρ^5 is strongly dependent on $\vartheta_2(\theta_2)$, reaching a maximum value of about 1.2 at the peaks of the cross section, and decreasing toward zero at its geometrical nodes. The overall corrective factor $\rho^5/(\rho_K^0\rho^6)$ is plotted in Fig. 6, along with the improved experimental cross section $\sigma^5_{\text{exp-imp}}$. The important question is now, does this correction restore the self-consistency of the normalization procedure? Actually, the best fit of Eq. (22) to $\sigma^5_{\text{exp-imp}}$ is obtained for $a_{\text{exp-imp}}=0.86$ kb/(eV$\times$sr^2), Γ being taken equal to 57°. The fivefold integration of Eq. (22) with these two parameters yields an ICS of 0.061 kb, which is still a factor 1.5 smaller than σ_K^0. So, despite the significant correction applied, which takes account of experimental resolution effects and culminates at about 1.8, the result of our consistency check remains negative when applied to $\sigma^5_{\text{exp-imp}}$. Clearly, another experimental effect still escapes the analysis. It is likely to be due to the small but finite dead time of the detector used in the experiment, under the specific conditions of coplanar geometry [38]. This is why we have decided to remedy the remaining inconsistency by roughly multiplying $\sigma^5_{\text{exp-imp}}$ by a global factor 1.5, thus obtaining what we call the consistent cross sections $\sigma^5_{\text{exp-cst}}$. The latter are the best estimates of the physical cross sections that can be extracted from the experiment considered.

C. Agreement between theory and renormalized experiment

Comparison between theory and experiment can then be performed in various ways.

The most usual one consists in comparing the raw theoretical FDCS, σ^5_{th}, with the best approximation of the latter that can be extracted from experiment, taking the current theory as a reference for normalizing the experiment, namely $\sigma^5_{\text{exp-norm}}=\sigma^5_{\text{exp-cst}}(\sigma^0_{\text{th}}/\sigma^0_K)$. This is done on the top row of Fig. 7, which demonstrates a remarkable agreement between theory and experiment on the absolute scale. Note how the improved normalization procedure restores the nodes in the experimental cross section, thus improving the agreement with the raw theoretical cross section, which shows exact nodes. The advantage of this approach is that it allows one to extract from experiment the quantities of physical interest, that is to say the cross sections, which are independent of every peculiarity of the experimental set-up. However, it does so using an approximate model of the FDCS (22). In this respect, a comparison between theory and experiment independent of any model might be still more relevant.

Such a comparison can be performed between averaged cross sections. We have thus averaged the theoretical cross section σ^5_{th} over the angular and energetic intervals relevant to the experiment Ref. [10] to get $\overline{\sigma}^5_{\text{th}}$. On the other side, Eqs. (19) and (23) can be used to define an averaged experimental cross section by

$$\overline{\sigma}^5_{\text{exp}} = \frac{\overline{\sigma}^0_K}{\Delta V^6}\frac{N^5}{N^0}. \tag{25}$$

The latter is then related to the experimental cross section of [10] by $\overline{\sigma}^5_{\text{exp}}=\sigma^5_{\text{exp}}/\rho^0\rho^6$. Before comparison with the theory, it must still be corrected for the unidentified experimental effects revealed in the previous section, which decrease the yield of events by a factor 1.5. It must also be renormalized to the current theoretical ICS σ^0_{th} instead of σ^0_K. The resulting averaged cross section, denoted by $\overline{\sigma}^5_{\text{exp-norm}}=\overline{\sigma}^5_{\text{exp}}1.5(\sigma^0_{\text{th}}/\sigma^0_K)$, which is nothing but $\sigma^5_{\text{exp-norm}}/\rho^5$, is displayed on the bottom row of Fig. 7. One sees that $\overline{\sigma}^5_{\text{th}}$ and $\overline{\sigma}^5_{\text{exp-norm}}$ are very close to each other on the absolute scale. Contrary to what was observed on the top row of the figure, the averaging of the theoretical FDCS now fills the exact nodes of the raw data, thus improving the agreement with the raw experiment. This comparison, opposite to the previous one, is independent of any model of the FDCS. Yet it concerns only averaged cross sections defined under particular experimental conditions. Note that the same approach was already used in Ref. [8], leading to outline the excellent agreement between theory and experiment, yet on the basis of a slightly different set of experimental data, anterior to those published in Ref. [10].

To conclude this section, let us point out that the agreement between theoretical and experimental *averaged* cross sections validates the theory, irrespective of any model. The *raw* cross sections of interest can therefore be taken from the theory with confidence. Finally, the agreement between theoretical and experimental *raw* cross sections validates the model-dependent renormalization procedure we have proposed in the previous section.

D. Discussion of Wannier's model of the FDCS

To complete this study of the fully differential cross section, let us now confront the assumptions underlying the expression (22) of the FDCS with what we can learn from the present *ab initio* calculations. The first of these assumptions is that the ungerade amplitude A_u in Eq. (17) is negligible with respect to its gerade counterpart A_g for all energy sharings. To test this hypothesis, we have calculated the ratio of the FDCS at $\vartheta_{12}=\pi$ to the peak value of the FDCS for a series of kinematics characterized by coplanar geometries and asymmetric sharings of the excess energy. This ratio, which gives an estimate of $|A_u/A_g|^2$, never exceeds a few percent. The second assumption states that A_g is independent of the energy sharing. In this respect, we have observed, while computing $\overline{\sigma}^5_{\text{th}}$, relative variations of the main (secondary) peak values of the FDCS of up to 10% (30%) as E_1/E described the interval [0,1]. As to the last assumption leading to Eq. (22), namely that A_g is a Gaussian function of the mutual angle with energy-dependent width and amplitude, it

simply cannot be tested against *ab initio* calculations regardless of the two previous ones. The present analysis thus confirms that Eq. (22) is a valuable first-order approximation. Yet it cannot account for every detail of the cross sections that nowadays experiments are able to distinguish. Accordingly, one should be prepared to observe very significant departures from the behaviors expected in this model. [Note, this is not at variance with the fact that we obtain satisfying fits of Eq. (22) to the theoretical cross sections, since any reasonable expression with enough build-in flexibility would do nicely.]

V. CONCLUSION

We have presented a full set of cross sections, ranging from the fully differential to the fully integrated one, for photodouble ionization of He at only 0.1 eV above the threshold. To our knowledge, there are only two previous *ab initio* studies of double escape in this near-threshold energy region: one of them, based on the propagating exterior complex scaling method, is devoted to electron impact ionization of H down to 0.01 a.u. above the threshold [7]; the other presents preliminary results obtained in the early stages of the present work [8]. This scarcity of the results reflects a major difficulty inherent in near-threshold studies, namely that a correlated dynamics prevails over distances that are very large, typically of the order of the inverse excess energy.

Despite their arduousness, such studies are essential to assess the relevance of the various pictures of the near-threshold dynamics which have emerged from previous model studies.

Care has therefore been taken to confront the present results with a series of forecasts regarding the differential cross sections, derived from the physical ideas outlined by Wannier in his pioneering study. As a result, these predictions are confirmed to provide valuable first-order approximations, it being understood that significant departures from the expected behaviors can be observed.

Photodouble ionization has also been approached as the limit of single ionization with excitation for infinitely high excitations. The present results, complementing those presented in the recent paper [9], suggest a new picture of this limit in the region close to the double ionization threshold, and call for further investigations.

Near-threshold studies are also very challenging for experimentalists: the cross sections are very low, which promises a very low counting rate; they vary rapidly with the excess energy, so that outstanding energy resolutions would be required to get more than an energy averaged information; the ejected electrons are very slow, which requires a perfect rejection of perturbing electric and magnetic fields. The agreement observed between the present results and the rare experiments available is therefore all the more remarkable. Regarding the fully differential cross sections, this agreement is obtained thanks to the changes we have introduced in the procedure that is currently used for normalizing the data from third-generation spectrometers. These changes might be of interest beyond the framework of the present study.

More generally, the present results, along with those presented in Ref. [9], demonstrate the ability of the H$\mathcal{R}$M-SOW method to provide a comprehensive view of the near-threshold dynamics, encompassing two- and three-body channels. In the near future, this method will be used to revisit the Wannier threshold law for the integrated cross section. We also plan to investigate the vicinity of the double ionization threshold from below.

ACKNOWLEDGMENTS

The authors acknowledge the support of the CNRS computer center IDRIS (Orsay, France) through the project 041485. They are grateful to A. K. Kazansky for useful discussions in the early stages of this work.

[1] J. S. Briggs and V. Schmidt, J. Phys. B **33**, R1 (2000).
[2] L. Malegat, in Proceedings of the XXIIIrd ICPEAC [Phys. Scr., T 110, 83 (2004)].
[3] T. Y. Shi and C. D. Lin, Phys. Rev. Lett. **89**, 163202 (2002).
[4] T. Schneider and J. M. Rost, Phys. Rev. A **67**, 062704 (2003).
[5] A. Y. Istomin, N. L. Manakov, and A. F. Starace, Phys. Rev. A **69**, 032713 (2004).
[6] G. H. Wannier, Phys. Rev. **90**, 817 (1953).
[7] Ph. L. Bartlett and A. T. Stelbovics, Phys. Rev. Lett. **93**, 233201 (2004).
[8] P. Selles, L. Malegat, and A. K. Kazansky, Inst. Phys. Conf. Ser. **183**, 141 (2004) (paper presented at the International Conference on Electron and Photon Impact Ionization and Related Topics, Louvain-la-Neuve, 2004).
[9] C. Bouri, P. Selles, L. Malegat, J. M. Teuler, M. Kwato Njock, and A. K. Kazansky, Phys. Rev. A **72**, 042716 (2005).
[10] A. Huetz and J. Mazeau, Phys. Rev. Lett. **85**, 530 (2000).
[11] G. C. King and L. Avaldi, J. Phys. B **33**, R215 (2000).
[12] L. Malegat, P. Selles, and A. K. Kazansky, Phys. Rev. Lett. **85**, 4450 (2000).
[13] P. Selles, L. Malegat, and A. K. Kazansky, Phys. Rev. A **65**, 032711 (2002).
[14] P. Selles, L. Malegat, P. Huetz, A. K. Kazansky, S. A. Collins, D. P. Seccombe, and T. J. Reddish, Phys. Rev. A **69**, 052707 (2004).
[15] L. Malegat, P. Selles, and A. K. Kazansky, in *Many Particle Quantum Dynamics in Atomic and Molecular Fragmentation*, edited by V. P. Shevelko and J. Ullrich (Springer Verlag, Heidelberg, 2003).
[16] U. Fano, and J. W. Cooper, Rev. Mod. Phys. **40**, 441 (1968).
[17] H. Friedrich, *Theoretical Atomic Physics* (Springer-Verlag, Berlin, 1991).
[18] M. Ya. Amusia, E. G. Drukarev, V. G. Gorshkov, and M. P. Kazachkov, J. Phys. B **8**, 1248 (1975).
[19] T. Suric and R. H. Pratt, J. Phys. B **37**, L93 (2004).
[20] G. C. King, M. Zubek, P. M. Rutter, F. H. Read, A. A. Mac-

Dowell, J. B. West, and D. M. P. Holland, J. Phys. B **21**, L403 (1988).
[21] F. H. Read, J. Phys. B **17**, 3965 (1984).
[22] F. H. Read and S. Cvejanovic, J. Phys. B **21**, L371 (1988).
[23] C. Bouri, P. Selles, L. Malegat, and M. G. Kwato Njock (unpublished).
[24] I. Vinkalns and M. Gailitis, *Abstract, 5th International Conference on the Physics of Electronic and Atomic Collisions* (Nauka, Leningrad, 1967).
[25] F. Peterkop, J. Phys. B **4**, 513 (1971).
[26] J. M. Rost, Phys. Rev. Lett. **72**, 1998 (1994).
[27] D. Proulx and R. Shakeshaft, Phys. Rev. A **48**, R875 (1993).
[28] M. Pont and R. Shakeshaft, J. Phys. B **28**, L571 (1995).
[29] G. Dawber, R. I. Hall, A. G. McConkey, M. A. MacDonal, and G. C. King, J. Phys. B **27**, L341 (1994).
[30] A. Huetz, P. Selles, D. Waymel, and J. Mazeau, J. Phys. B **24**, 1917 (1991).
[31] F. Maulbetsch and J. S. Briggs, Phys. Rev. Lett. **68**, 2004 (1992).
[32] R. Wehlitz, F. Heiser, O. Hemmers, B. Langer, A. Menzel, and U. Becker, Phys. Rev. Lett. **67**, 3764 (1991).
[33] C. H. Greene, J. Phys. B **20**, L357 (1987).
[34] H. Kossmann, V. Schmidt, and T. Andersen, Phys. Rev. Lett. **60**, 1266 (1988).
[35] J. M. Bizau and F. J. Wuileumier, J. Electron Spectrosc. Relat. Phenom. **71**, 205 (1995).
[36] L. Malegat, P. Selles, and A. Huetz, J. Phys. B **30**, 251 (1997).
[37] We call "coplanar" a geometry in which the two electrons and the electric field of the linearly polarized photon beam are in the same plane.
[38] A. Huetz (private communication).
[39] H. Braüning, R. Dörner, C. L. Cocke, M. H. Prior, B. Krässig, A. S. Kheifets, I. Bray, A. Braüning-Demian, K. Carnes, S. Dreuil, V. Mergel, P. Richard, J. Ullrich, and H. Schmidt-Böcking, J. Phys. B **31**, 5149 (1998).
[40] The magic angle ϑ_M is defined by $P_2(\cos\vartheta_M)=0$, P_2 being the second-order Legendre polynomial.